Reticulated Lipid Probe Fluorescence Reveals MDCK Cell Apical Membrane Topography

Pina Colarusso and Kenneth R. Spring
Laboratory of Kidney and Electrolyte Metabolism, National Heart, Lung, and Blood Institute, National Institutes of Health, Bethesda, Maryland 20892-1603, USA

ABSTRACT High spatial resolution confocal microscopy of young MDCK cells stained with the lipophilic probe 1,1′-dihexadecyl-3,3,3′,3′- tetramethylindocarbocyanine perchlorate ($DiIC_{16}$) revealed a reticulated fluorescence pattern on the apical membrane. $DiIC_{16}$ was delivered as crystals to live cells to minimize possible solvent perturbations of the membrane lipids. The ratio of the integrated fluorescence intensities in the bright versus dim regions was 1.6 ± 0.1 ($n = 13$). Deconvolved images of the cells were consistent with exclusive plasma membrane staining. Multi-spectral and fluorescence anisotropy microscopy did not reveal differences between bright and dim regions. Bright regions coincided with microvilli and microridges observed by differential interference contrast microscopy and were stable for several minutes. Fluorescence recovery after photobleaching yielded similar diffusion coefficients (pooled $D = 1.5 \pm 0.6 \times 10^{-9}$ cm^2/s, $n = 40$) for both bright and dim regions. Line fluorescence recovery after photobleaching showed that the reticulated pattern was maintained as the fluorescence recovered in the bleached areas. Cytochalasin D did not affect the staining pattern, but the pattern was eliminated by cholesterol depletion with methyl-β-cyclodextrin. We conclude that the reticulated fluorescence pattern was caused by increased optical path lengths through the microvilli and microridges compared with the flat areas on the apical membrane.

INTRODUCTION

MDCK cells are large and flat in the early stages after seeding as they spread to form a confluent monolayer. Such young cells allow for the clear visualization of apical membrane features that may be more difficult to observe in the smaller and more closely packed mature cells. In a previous study, for example, a punctate binding pattern of the lectin wheat germ agglutinin was observed in the apical membrane of young MDCK cells (Kovbasnjuk and Spring, 2000). The lectin binding sites were thought to denote individual proteins or protein clusters. As the cells matured and grew taller, lectin binding became more dense and uniform, and individual points became difficult to detect. These results led us to question whether other markers, such as fluorescent lipid probes, also would reveal nonuniform distributions that might be obscured in older cells.

The long chain indocarbocyanines, designated $DiIC_n$ ($n = 12, 14, 16\ldots$), are standard fluorescent probes for the investigation of membrane structure and function. These lipid analogues are amphiphilic, consisting of a polar head group connecting two alkyl chains. In mammalian cells, $DiIC_n$ molecules are thought to be embedded in the outer leaflet of the plasma membrane with the head groups parallel to the cell surface and the alkyl tails parallel to the endogenous phospholipid acyl chains (Axelrod, 1979; Wolf, 1985). When examined with widefield or confocal microscopy, $DiIC_n$ probes generally have been reported to label the plasma membrane uniformly with perhaps minor variations in intensity. We observed, however, that confocal imaging of the apical membrane of young MDCK cells revealed distinct reticulated 1,1′-dihexadecyl-3,3,3′,3′-tetramethylindocarbocyanine perchlorate ($DiIC_{16}$) labeling on the scale of a few hundred nanometers. As the origin of such brightness variations had not been thoroughly investigated, we undertook a systematic analysis of the labeling of the plasma membrane in MDCK cells with $DiIC_{16}$ and related probes.

The reticulated $DiIC_n$ staining pattern of the apical membrane may arise from dye partitioning or hindered diffusion associated with regional differences in lipid composition or protein organization. For example, regions containing clusters of acetycholine receptors are enriched in $DiIC_{12}$ and $DiIC_{18}$ relative to acetycholine poor areas in myotube plasma membranes (Scher and Bloch, 1991). It has also been reported that cross-linking of immunoglobulin E receptors leads to a heterogeneous distribution of $DiIC_{16}$ in the plasma membrane of red blood cells (Thomas et al., 1994). In addition, heterogeneous probe labeling due to chemical differences would have implications for the lipid raft hypothesis, which proposes the existence of specialized lipid microdomains with dimensions of tens of nanometers, well below the spatial resolution limit of conventional fluorescence microscopy (Jacobson and Dietrich, 1999).

Another explanation for the observed fluorescence intensity differences are changes in physical properties unrelated to lipid distribution, such as membrane geometry. Because the transition dipole of $DiIC_n$ lies nearly parallel to the

Submitted August 20, 2001, and accepted for publication October 11, 2001.

Address reprint requests to Pina Colarusso, National Institutes of Health, Building 10, Room 6N260, 10 Center Drive, Bethesda, MD 20892-1603. Tel.: 301-402-4719; Fax: 301-402-1443; E-mail: colarusp@nhlbi.nih.gov.

0006-3495/02/02/752/10 $2.00

plasma membrane, polarized light microscopy yields different fluorescence intensities arising from changes in membrane orientation (Axelrod, 1979; Sund et al., 1999). Indeed, intensity differences can be observed along the edges of specimens with well-defined geometry, such as red blood cell ghosts (Axelrod, 1979) or yeast cells (Greenberg and Axelrod, 1993). However, intensity differences due to orientation are easily obscured in samples with irregular geometries and slowly varying membrane curvature. This poorer discrimination applies both to standard epi- or transillumination; it is noteworthy that total internal reflection fluorescence microscopy in many cases provides much better contrast between different membrane orientations (Sund et al., 1999).

The reticulated fluorescence pattern also could be due to variations in the optical path along the apical surface of MDCK cells. The proportion of membrane contained in the optical path changes along the apical surface because the membrane is folded into microvilli or microridges (microplicae). The increase in the membrane optical path created by these topographical features could result in the excitation of more dye molecules, thus producing more intense localized emission. Internalization of dye molecules in regions very close to the plasma membrane would also yield increased intensities because the dye both on surface and internal membranes would then be contained in the optical path.

We have examined the origin of the nonuniform lipid probe fluorescence in the MDCK plasma membrane using several approaches. These include measurements of dye diffusion coefficient to determine if there were local restrictions to dye mobility, digital deconvolution to examine whether the probe was confined to the plasma membrane, fluorescence anisotropy to determine whether dipole orientation was the source of intensity differences, and multispectral microscopy to ascertain whether regional differences in the microenvironment altered the dye emission spectra. We also examined the effect of cytoskeleton disruption by cytochalasin D and cholesterol depletion by methyl-β-cyclodextrin on the $DiIC_{16}$ distribution.

A crucial observation was that the bright areas in the reticulated $DiIC_{16}$ fluorescence corresponded to surface ridges simultaneously observed using high-resolution differential interference contrast (DIC) microscopy. Furthermore, the intensity differences between the bright and dim areas could be explained by variations in the membrane optical path length associated with the microridges. Finally, we observed that MDCK cells treated with the cholesterol sequestering agent methyl-β-cyclodextrin exhibited uniform fluorescence on the apical surface, whereas the simultaneous DIC images revealed a greatly reduced number of microridges and microvilli. Our findings highlight the importance of surface membrane topography in the interpretation of the distribution of fluorescent lipid probes.

MATERIALS AND METHODS

Cell culture

Wild-type MDCK cells (passages 64–76 from the American Type Culture Collection, Rockville, MD) were grown on glass coverslips (25-mm diameter) in Dulbecco's modified Eagle medium containing 10% bovine serum and 2 mM glutamine. The Dulbecco's modified Eagle medium did not contain antibiotics, riboflavin, or phenol red.

Cell perfusion

All experiments were carried out on live cells (3–8 days after seeding) maintained in a temperature-controlled perfusion chamber in which the composition and flow of the perfusate were controlled by computerized pinch valves (Harris et al., 1994). Cells were continuously perfused with medium containing 142 mM Na^+, 5.3 mM K^+, 1.8 mM Ca^{2+}, 0.8 mM Mg^{2+}, 14 mM HEPES, 136.9 mM Cl^-, 0.8 mM SO_4^{2-}, and 5.6 mM glucose (pH adjusted to 7.4 at 21–23°C).

Fluorescence labeling

All fluorescent probes were purchased from Molecular Probes (Eugene, OR). $DiIC_{16}$ was dissolved in ethanol (10 mg/mL) and stored in the dark at 4°C. Just before labeling, the ethanolic $DiIC_{16}$ solution was diluted 1000-fold in HEPES buffer while vigorously mixing. The cells were perfused with the dye solution for 1 to 5 min, and then the perfusion solution was switched back to the HEPES buffer. Similar procedures were used to label the cells with Fast- DiI (1,1′-dilinoleyl-3,3,3′,3′- tetramethylindocarbocyanine, 4-chlorobenzenesulfonate), $DiIC_{12}$, 5-hexadecafluor (5-hexadecanoylaminofluorescein), and FM1–43 (N-(3-triethylammoniumpropyl) -4-(4-(dibutylamino)styryl) pyridinium dibromide). Experiments were carried out between 21 to 23°C to minimize dye internalization. In addition, fluorescence emission spectra of $DiIC_{16}$ dissolved in absolute ethanol or HEPES buffer were recorded at 2-nm resolution (Fluoromax-2 spectrometer; Spex Industries, Edison, NJ).

Differential interference contrast and fluorescence microscopy

Confocal images (100×/1.3 N.A. oil immersion objective) were acquired on an inverted epifluorescence microscope (Nikon, Mellville, NY) coupled to a laser scanning unit (Odyssey, Noran, Middleton, WI). Simultaneous DIC images were recorded as previously described (Spring, 1990). The excitation wavelength was selected from the multimode output of an argon ion laser by an acousto-optic tunable filter, which also served as a variable attenuator. Fluorescence was excited at 488 nm and detected at wavelengths longer than 515 nm. Wavelength-resolved images were also acquired by placing a liquid crystal tunable filter (LCTF) in the detection path. Images were integrated for 64 or 128 frames at a rate of 30 frames/s and were digitized at 8-bit resolution. All digital images in this report were prepared using MetaMorph Version 4.6 (Universal Imaging Corporation, West Chester, PA).

Deconvolving and sharpening images

To remove out-of-focus fluorescence, stacks of confocal optical sections were deconvolved using a full iterative method (EPR, Scanalytics, Vienna, VA). The experimental point-spread function was determined by recording the corresponding sections through sub-resolution (0.1-μm diameter) fluorescent beads (Molecular Probes). The reconstructed images were then checked for consistency by comparison with the results of unsharp mask processing.

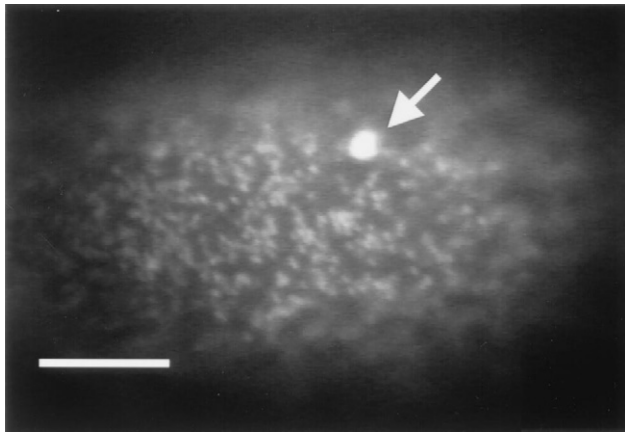

FIGURE 1 A confocal section showing a reticulated fluorescence pattern in the apical membrane of an MDCK cell. The arrow indicates a $DiIC_{16}$ crystal. Scale bar = 10 μm.

Fluorescence recovery after photobleaching experiments

Two types of fluorescence recovery after photobleaching (FRAP) experiments were carried out: spot and line FRAP. In spot FRAP, a 0.45-μm beam radius spot was positioned on a fluorescent region of the apical surface of a MDCK cell. The time course was as follows: 3-s prebleach probe, 0.1- to 0.2-ms bleach, and 5-s recovery probe. Data points were collected every 10 ms. Typically, the bleach pulse was 1000× more intense than the monitoring beam; the laser power was varied by the acousto-optic tunable filter at the laser output. All experiments were carried out between 21 and 23°C. The data were analyzed using a radial diffusion model (Axelrod et al., 1976). Line FRAP measurements were performed by bleaching a 0.45 × 3 μm area for 1.5 to 2 s and monitoring the fluorescence recovery at 2-s intervals.

Cholesterol depletion and cytoskeleton disruption

To deplete membrane cholesterol, MDCK cells were incubated at 37°C with 20 mM methyl-β-cyclodextrin in HEPES buffer (pH 7.4, 290–310 mOsm) for 120 min before labeling in the perfusion chamber. In the cytoskeletal disruption experiments, the cells were either incubated or perfused with HEPES buffer containing 1.8 μM cytochalasin D (Sigma, St. Louis, MO) dissolved in DMSO (3 mg/ml) for times ranging between 10 and 60 min at 37°C. Once the cells were treated with either reagent, labeling with $DiIC_{16}$ was carried out as described above.

RESULTS

Reticulated staining pattern

Examination of cells labeled with $DiIC_{16}$ with a confocal microscope at high magnification revealed a reticulated pattern of fluorescence on the apical surface; a typical image is shown in Fig. 1. We were concerned that delivering a fluorescent probe with a lipophilic carrier might alter the membrane lipids and create an artifactual pattern; therefore, we developed a technique to deliver solvent-free crystals of $DiIC_{16}$ to the apical membrane. An ethanolic stock solution of $DiIC_{16}$ diluted in HEPES buffer (ethanol concentration <0.1%) was vortexed to yield a suspension of micron-sized crystals. When the apical surface of the monolayer was briefly perfused with this dye solution, single crystals adhered to the apical membrane of some cells. The number of labeled cells was determined by the duration of dye exposure. Membrane labeling occurred as the dye molecules diffused from the adherent crystal through the lipids of the plasma membrane (Fig. 2).

$DiIC_{16}$ diffusion

The diffusion of $DiIC_{16}$ from the adherent crystal over the entire apical membrane of a typical cell occurred within a few minutes; Fig. 2 (*top*) displays two images recorded 36 s apart. The reticulated pattern appeared as the dye molecules diffused over the apical region. The probe also was seen to diffuse from the crystal on the apical surface to the lateral and basal membranes. The diffusion coefficient of $DiIC_{16}$ in the apical membrane at 21 to 23°C was determined by spot FRAP to be $1.5 \pm 0.6 \times 10^{-9}$ cm^2/s ($n = 40$). The data were analyzed using nonlinear fit to a model describing two-dimensional recovery of a beam with a Gaussian profile (Axelrod et al., 1976). The bright and dim areas did not exhibit significant differences in either the diffusion constant (bright, $1.3 \pm 0.5 \times 10^{-9}$ cm^2/s, $n = 11$; dim, $1.8 \pm 0.5 \times 10^{-9}$ cm^2/s, $n = 6$) or mobile fraction (over 90% for both). Furthermore, a qualitative examination of line FRAP experiments showed that fluorescence recovered in its original pattern. We conclude, therefore, that the reticulated staining pattern was not caused by differences in probe mobility in the bright and dim regions.

The value for diffusion coefficient that was obtained with spot FRAP was checked by examining the spatial profile of $DiIC_{16}$ fluorescence as a function of time. The middle panels in Fig. 2 show linear fluorescence profiles with the crystal center as the origin, which were extracted from a time series of images obtained as the dye diffused through the plasma membrane. Fig. 2 (*bottom panel*) shows an example of a time series of the fluorescence profiles and the curve fit to the solution for the diffusion equation for a constant concentration reservoir in a semiinfinite medium (Crank, 1979):

$$C = C_0 \,\mathrm{erfc}[r/2(Dt)^{1/2}], \quad (1)$$

in which C is the concentration of the $DiIC_{16}$, r is the distance to the center of the crystal, D is the diffusion coefficient, and t is the elapsed time. This method of analysis gave an area averaged $D = 2.3 \pm 0.7 \times 10^{-9}$ cm^2/s ($n = 5$), which is not significantly different from the value obtained with spot FRAP experiments.

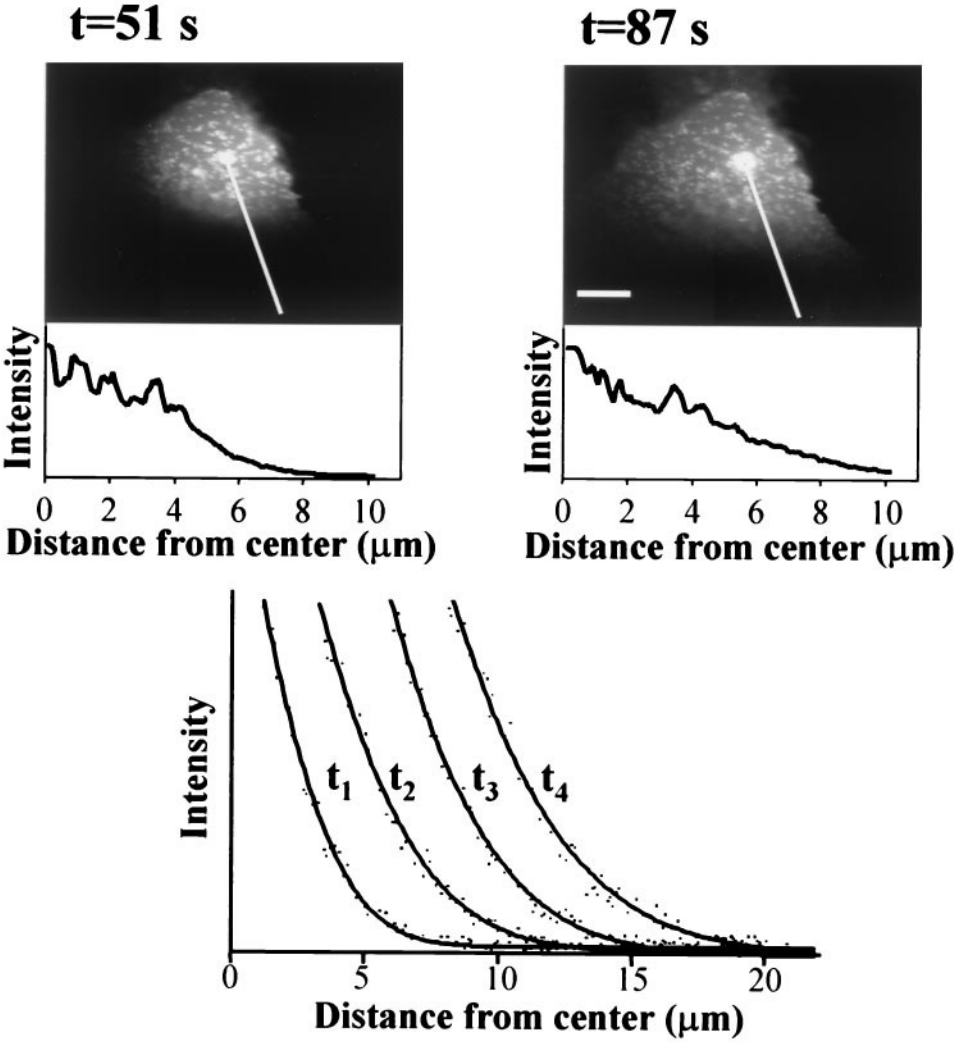

FIGURE 2 (*Top*) Two images recorded 36 s apart showing the diffusion of $DiIC_{16}$ from an adherent crystal into the lipid bilayer of the apical membrane of an MDCK cell. Scale bar = 5 μm. The middle panels illustrate the fluorescence intensity profiles originating from the crystal center along the lines indicated in the upper images. The bottom panel shows data points (*dots*) at four time points (t_1 = 13 s, t_2 = 32 s, t_3 = 50 s, t_4 = 72 s) and the corresponding fit (*solid lines*) to a diffusion model described in the text.

Deconvolution confirms plasma membrane localization

We were concerned that the reticulated $DiIC_{16}$ pattern could be the result of rapid regional internalization of fluorescently labeled membrane that remained close to the plasma membrane. To improve the *z*-axis discrimination of the stained regions, the confocal images were further processed using digital deconvolution. This was necessary for the best views of the apical membrane because the images, although obtained with a confocal microscope, were still degraded by light from out-of-focus planes. Stacks of confocal images were recorded at 0.1-μm focus increments and were deconvolved using a full iterative method. The reconstructed stacks showed a fluorescence pattern consistent with staining confined to the plasma membrane. The validity of the deconvolved images was confirmed by the application of unsharp masking, another image processing method used to reduce out-of-focus fluorescence.

Optical sectioning showed that preconfluent as well as confluent cells both exhibited staining of both the apical and basal membranes. Representative deconvolved sections from the apical, middle, and basal portions of the cell are given in Fig. 3 (*a–c*). The apical membrane exhibits a reticulated distribution of light and dim areas. Because the apical surface of MDCK is curved, the various features are in focus in different optical sections. The dim areas did not fill in when the confocal sections through the apical membrane were superimposed. Fig. 3 *b* shows the staining of the lateral membrane, which also displays variations in the fluorescence intensity. In Fig. 3 *c*, the staining is seen to

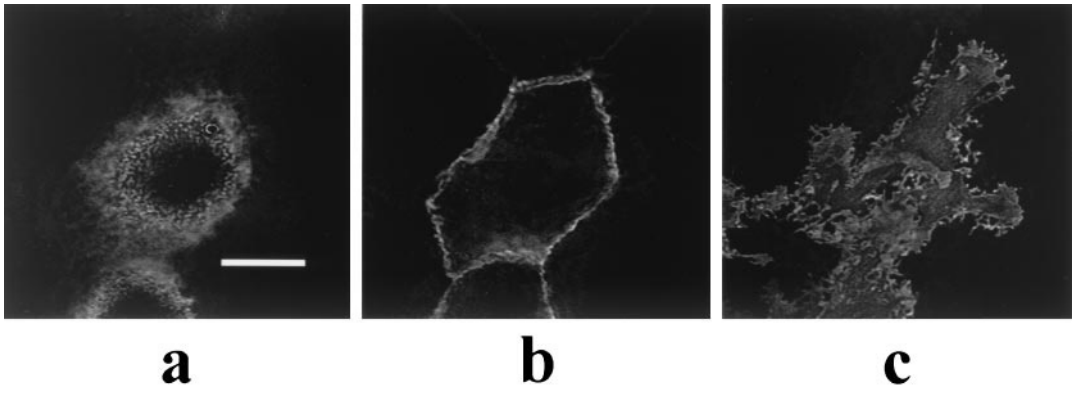

FIGURE 3 Deconvolved images of $DiIC_{16}$ labeling of the apical (*a*), lateral (*b*), and basal membrane (*c*) in an MDCK cell. Reticulated $DiIC_{16}$ fluorescence is visible in the apical membrane. Scale bar = 10 μm.

form an intricate, convoluted pattern that traces the basal membrane domain of the cell.

Time stability

The reticulated pattern on the apical membrane was stable on the order of minutes. As shown in Fig. 4, surface features remained in the same configuration for at least 3 minutes. The correspondence was within the experimental error arising from changes in cell shape as well as to the mechanical instabilities in the perfusion chamber and the microscope. These experimental factors also precluded monitoring the cells for longer time periods. The stability of the pattern is consistent with a structural basis for the reticulated pattern.

Other fluorescent lipid probes

The apical membrane of both preconfluent and confluent cells also was stained heterogeneously by other lipidic dyes such as $DiIC_{18}$, $DiIC_{12}$, 5-hexadecafluor, and FM1–43. All the DiI analogs showed plasma membrane labeling similar to $DiIC_{16}$ with the exception of Fast-DiI. Fast-DiI showed

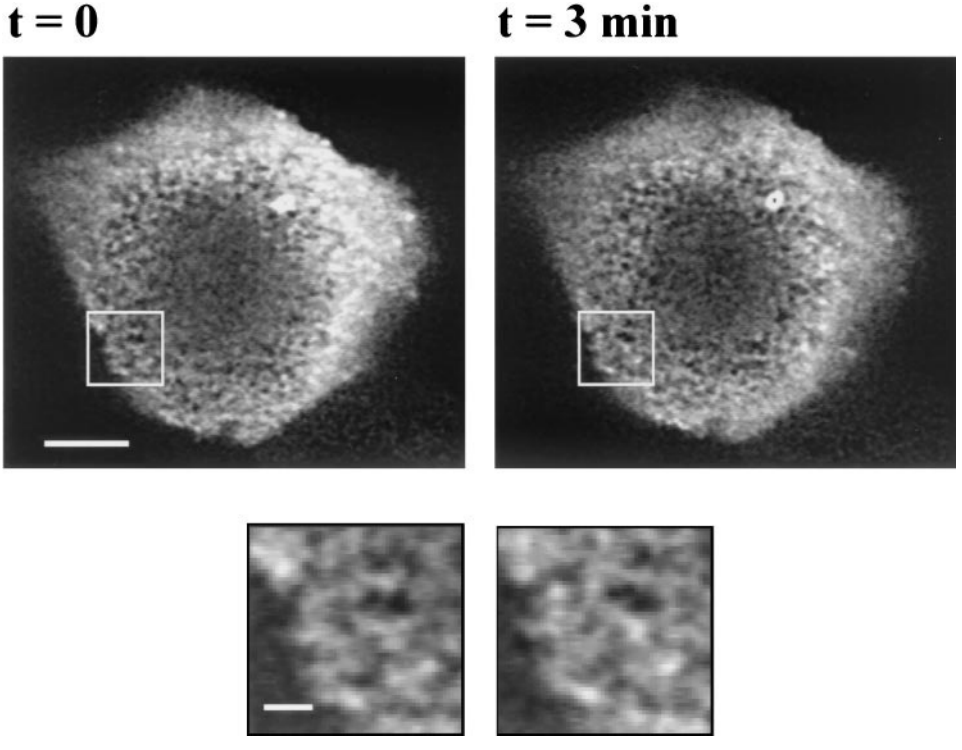

FIGURE 4 Time stability of the reticulated $DiIC_{16}$ fluorescence pattern on the apical membrane of MDCK cells. The two confocal sections were recorded 3 min apart. Upper scale bar = 5 μm; lower scale bar = 1 μm.

weak apical plasma membrane fluorescence as well as substantial internalization with formation of bright structures that interfered with the observation of plasma membrane labeling. Unlike the other DiI analogues examined in these experiments, Fast-DiI did not stain the lateral or basolateral membranes of confluent MDCK cells.

$DiIC_{16}$ was delivered to the cells more effectively than the more lipophilic $DiIC_{18,}$ which tended to aggregate and precipitate out of the perfusate. In addition, $DiIC_{16}$ exhibited minimal internalization over the time course of the experiments (~30–60 min). $DiIC_{12}$, in contrast, was readily internalized and showed diffuse cytoplasmic staining in addition to the plasma membrane labeling within a few minutes. We conclude that probes that remain in the plasma membrane, such as the long-chain DiI analogs, all exhibit a similar reticulated staining pattern and that dye internalization could be identified and eliminated as the cause of the reticulated $DiIC_{16}$ pattern.

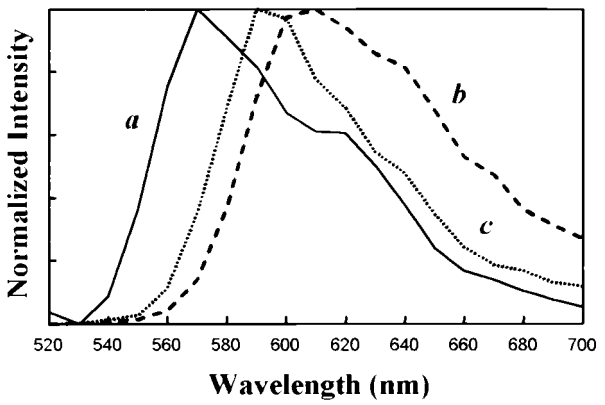

FIGURE 5 Normalized spectra of $DiIC_{16}$ emission recorded from the cell surface using a LCTF on the confocal microscope: (*a*) the bright and dim areas within the apical membrane of MDCK cells; (*b*) $DiIC_{16}$ crystals; (*c*) intermediate between *a* and *b*. Excitation $\lambda = 488$ nm.

Dipole orientation and membrane staining

Experiments were carried out to determine whether the reticulated pattern resulted from the orientation of the dye molecule dipole on the apical surface of MDCK cells. It has been shown that the DiI transition dipole is aligned nearly parallel to the plane of the membrane in red cell ghosts (Axelrod, 1979). It is probable that $DiIC_{16}$ is similarly oriented in the apical membrane of MDCK cells. To investigate whether the reticulated pattern was a polarization artifact, anisotropy measurements were made using an LCTF in the emission path of the microscope (Spring, 2000). The transmission of the LCTF may be varied according to the polarization of detected fluorescence. Images recorded parallel and perpendicular to the excitation polarization did not exhibit significant differences in fluorescence intensity or pattern. The ratio of the bright to dim areas was 1.6 ± 0.2 and 1.7 ± 0.2 for the vertical and horizontal polarizations, respectively ($n = 5$). In addition, no changes were observed when the laser excitation beam was depolarized with a quarter-wave plate. It is unlikely, therefore, that differences in dye dipole orientation were the source of the reticulated pattern.

Spectral investigations

If the bright and dim regions correspond to different chemical microenvironments, the $DiIC_{16}$ emission spectrum might show some variations between the bright and dim regions. To this end, the fluorescence emission was imaged between 520 to 700 nm at 10-nm wavelength intervals with the LCTF. Spatially resolved spectra thus were available for each image pixel. The imaging data sets were divided by intensity thresholding into bright and dim areas, and the signal was averaged for both the bright and dim pixel populations. Once the intensities were normalized, the emission spectra were identical in the bright and dim regions, at least to the limit of the spectral resolution available with the LCTF. Most of the spectra associated with the apical membrane (>99%) resembled the solid trace labeled *a* in Fig. 5. The spectra are consistent with the $DiIC_{16}$ molecules in the bright and dim areas experiencing a similar chemical microenvironment.

Although the spectra of the bright and dim regions were identical, variations were observed in the spectra of the $DiIC_{16}$ crystals on the cell surface. The spectra of the dye crystals resembled either trace Fig. 5 (*a* or *b*); the relative maxima are separated by ~40 nm. To help in the assignment, bulk spectra were recorded of $DiIC_{16}$ dissolved either in ethanol or HEPES buffer (excitation $\lambda = 488$ nm). Spectrum *a* closely resembled the trace obtained for $DiIC_{16}$ dissolved in ethanol, whereas spectrum *b* matched that of $DiIC_{16}$ suspended in HEPES buffer. These two solvents approximate the less polar lipid environment of the apical membrane and the polar HEPES perfusate, respectively. These results lead to the assignment of the two observed spectral classes as $DiIC_{16}$ dissolved in the plasma membrane *a* or in the buffer solution *b*. Spectrum *c* is intermediate between *a* and *b*; this signature represents a mixture of the two pure component spectra, and as expected, could be observed at the boundaries of the dye crystals that were gradually diffusing into the surrounding lipid environment.

DIC images of the apical membrane

To determine whether there was a structural basis for the reticulated pattern, we examined the spatial relationship of the reticulated fluorescence pattern to the microridges and microvilli on the apical membrane surface that were visible with simultaneous DIC imaging. When the pattern of bright

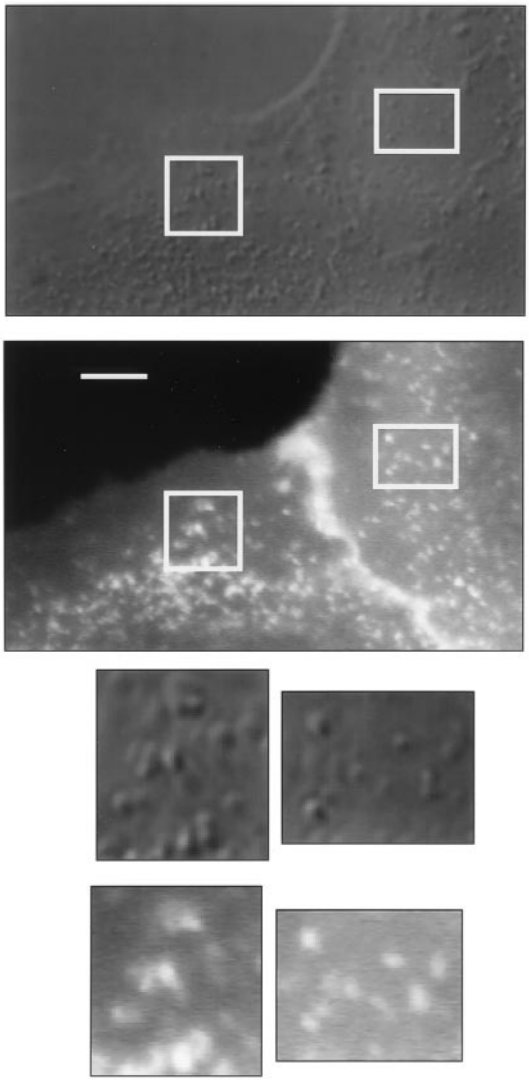

FIGURE 6 Corresponding DIC (*upper*) and fluorescence images (*lower*). The bright areas in the fluorescence images correspond to surface features in the DIC images. Scale bar = 5 μm.

and dim regions of $DiIC_{16}$ fluorescence was superimposed on high-resolution DIC images of the apical surface, it became evident that the bright regions corresponded to elevations of the surface. An example of the comparison of the fluorescence and DIC images is shown in Fig. 6.

A similar correspondence was observable with the lipid probe 5-hexadecafluor. From these results we inferred either that the probe distribution was different in the elevated regions or that more membrane was contained in the optical path due to the surface geometry. Because the diffusion and multispectral imaging experiments failed to show any chemical differences between bright and dim areas, we directed our efforts to determining whether the intensity differences were the result of irregularities in surface contours.

Cholesterol depletion

Cholesterol depletion has been reported to not only alter apical membrane lipid composition but also to smooth the apical membrane and reduce the size of the surface ridges and projections (Francis et al., 1999). $DiIC_{16}$ labeling was examined after depleting cholesterol from the plasma membrane with methyl-β-cyclodextrin. The cells were incubated with 20 mM of the cholesterol acceptor for 2 h in a HEPES buffer. After the cholesterol depletion, almost all of the labeled cells showed uniform fluorescence, as shown in Fig. 7. In addition, the cells were more rounded, their lateral membrane appeared less interdigitated, and the normally highly convoluted basolateral membrane pattern was not observed. In the corresponding DIC images, the apical surface was smooth with sparser and less prominent surface ridges and more apical surface pitting. Because the cyclodextrin addition to the HEPES buffer increased the osmolality by 20 mOsm, the experiments were repeated in solutions with a compensatory reduction in the NaCl concentration to maintain the osmolality of 290 mOsm.

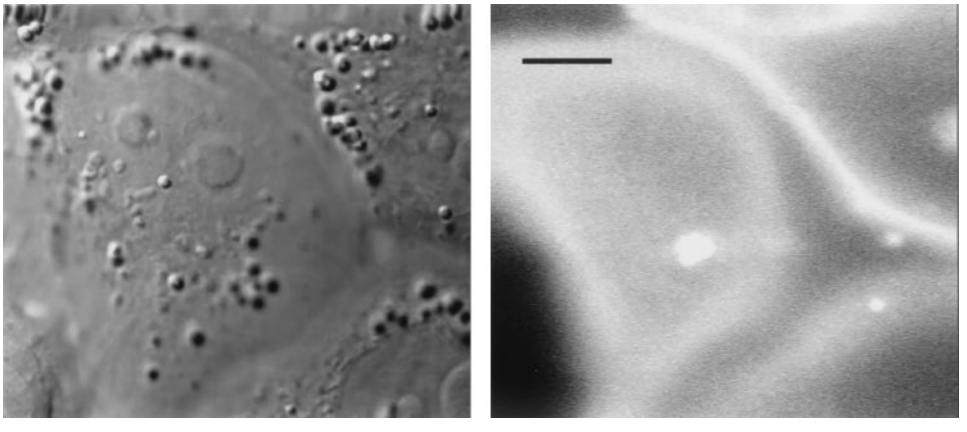

FIGURE 7 Methyl-β-cyclodextrin treatment of MDCK cells. After 2 h, the microridges and microvilli in the DIC images (*left*) are not visible with an accompanying smoothing of the fluorescence intensities (*right*). Scale bar = 5 μm

Both conditions yielded identical results. Therefore, cholesterol depletion eliminated both the reticulated staining pattern and the surface irregularities that characterized untreated cells. Two explanations are consistent with these observations: the differences in probe distribution could be related to the respective cholesterol content in the bright and dim regions, or the loss of surface structures could be the basis for the development of uniform fluorescence.

Measurements using spot FRAP showed that the diffusion coefficient for $DiIC_{16}$ in the apical membrane was not significantly altered by cholesterol depletion. The mean $\pm$ SD for the diffusion coefficient was $1.8 \pm 0.7 \times 10^{-9}$ cm^2/s, $n = 6$. Moreover, spectral curves of cholesterol-depleted cells whose membranes had been stained with $DiIC_{16}$ did not differ from those of control cells. Thus, we conclude that the presence of cholesterol in the apical membrane did not impede the diffusion of $DiIC_{16}$ in the bilayer or interact with the probe to alter its microenvironment. We, therefore, concentrated our efforts on the effects of the membrane topography on the fluorescence.

Membrane topography and fluorescence intensity

Our microscope, similar to other confocal apparatus, has an axial resolution limit of ~ 0.8 μm, which was not sufficient for optical sectioning of the microvilli and microridges. It is possible then that fluorescence emission appeared more intense at the microvilli and microridges because the optical paths through these protrusions contained more membrane. If this were indeed the origin of the reticulated fluorescence intensity distribution, the fluorescence ratio of the bright to dim regions should be related to the surface area ratio of the membrane protrusions to their projections in two dimensions.

On the simplest level, the microvillus can be modeled as a hemisphere. The ratio of the surface area of a hemisphere to the circle corresponding to its two-dimensional projection is 2. This value is in reasonable agreement with the experimental value of 1.6 ± 0.1. A more comprehensive model has also been developed for the microvillus surface. Although determining an analytical expression that describes the exact shape of a nonplanar membrane is a complex task, an approximation was developed that represents the microvillus membrane surface, Z, by a periodic function (Aizenbud and Gershon, 1982)

$$Z = A \cos 2\pi l_x^{-1} x \cos 2\pi l_y^{-1} y, \quad (2)$$

in which A = microvillus height and l_x and l_y are the unit cell dimensions along x and y. Each unit cell contains one microvillus. The surface area (S.A.) of the membrane is given by

$$\text{S.A.} = \int\int [1 + (dZ/dx)^2 + (dZ/dy)^2]^{1/2} dx dy. \quad (3)$$

The ratio of the surface area of a microvillus to the area of the unit cell can be determined numerically. This ratio should predict the ratio of the fluorescence intensities between the membrane protrusions to the flat regions. However, the finite lateral spatial resolution of the imaging system must be considered when performing these calculations. To illustrate, consider an isolated microvillus with $A = 0.2$ μm and $l_x = l_y = 0.1$ μm, dimensions comparable with those of cortical collecting duct cells in the rat kidney (Andrews and Porter, 1974). From Eq. 3, the microvillus S.A. is computed to be 0.0858 μm^2, whereas its projected surface area is equal to 0.01 μm^2, the unit cell area given by l_x. l_y. Because the lateral spatial resolution limit of our imaging system is 0.24 μm, it follows that the fluorescence from a 0.1×0.1 μm unit cell would be detected over a region ranging from 0.24×0.24 μm^2 to 0.48×0.48 μm^2, depending on whether the center of a microvillus was located at the center or on a corner of a pixel, respectively. Taking the spatial resolution into account, the corrected S.A. is then the sum of the computed microvillus area and the difference between detection region area and that of the unit cell. For this example, the ratio between the corrected S.A. of the microvillus to that of the detection region ranges between 1.3 and 2.3. Similarly, for a microridge with width 0.1 μm and length 1 μm, the corrected surface area would yield an increased fluorescence between a factor 1.6 to 2.5 for the microridge compared with the flat membrane. These values are in agreement with our experiments, in which the integrated fluorescence intensity between the bright and dim regions was found to be 1.6 ± 0.1 ($n = 13$). Thus, we conclude that the increased membrane optical path resulting from the convoluted apical surface is the likely basis of the reticulated fluorescence pattern.

Reticulated pattern does not require an intact cytoskeleton

The role of the actin cytoskeleton in the formation or maintenance of the reticulated pattern was investigated by treating the cells with cytochalasin D before labeling them with $DiIC_{16}$. The cells were subjected to a 60-min incubation with 1.8 μM cytochalasin D in HEPES buffer. This dosage was based on published work with MDCK cells in which 1.8 μM cytochalasin D was sufficient to disrupt the F-actin organization of the terminal web and actin-myosin circumferential ring in MDCK cells (Kovbasnjuk et al., 1998). In our experiments, the cells became more susceptible to deformation by the flowing perfusate, but the reticulated fluorescence pattern and the associated microridges were unaffected. A DMSO control was also indistinguishable from the untreated cells. The relative area of the apical membrane occupied by bright regions in the reticulated pattern, determined from intensity thresholding the images, is a direct measure of the extent of the surface ridges. Treatment with 1.8 μM cytochalasin D did not significantly

alter the relative areas of the bright and dim regions (percentage of area of bright regions: control = 33.4 ± 5.9, n = 9; cytochalasin = 37.5 ± 2.7, n = 9). We conclude that disruption of the actin cytoskeletal anchorage of proteins or membrane does not affect the structural integrity of the individual microridges on the apical surface of MDCK cells.

DISCUSSION

The goal of this investigation was determination of the origin of the reticulated $DiIC_{16}$ fluorescence pattern on the apical membrane of MDCK cells. We concluded that the microvilli and microridges, visible in MDCK cells using high-resolution DIC microscopy, fluoresced more brightly with $DiIC_{16}$ than did the surrounding areas because of their increased optical path length rather than regional differences in microenvironment of the probe. Indeed, modeling the membrane protrusions using a geometric approach yielded a ratio that was consistent with the experimentally observed relative intensity ratios. We think that the $DiIC_{16}$ staining pattern may prove a useful measure of membrane surface topography and may aid in localizing proteins to specific regions on the plasma membrane.

Recent investigations have suggested that protein-lipid interactions, primarily those involving cholesterol, are different in the microvillar and planar regions in the apical membrane in MDCK cells (Corbeil et al., 1999; Snyers et al., 1999; Roper et al., 2000). Although it is possible that $DiIC_{16}$ partitions into different chemical environments in the microvilli, we could not resolve any possible nonuniformities within these regions because the reticulated pattern is on the order of the spatial resolution of our imaging system (~0.24 μm lateral). Analyses by FRAP and spectral scanning did not reveal differences in the chemical microenvironment on these length scales. No significant differences were found between the bright and dim areas in either the lateral diffusion constant or mobile fraction of $DiIC_{16}$. This finding is consistent with other work that finds slight, if any, dependence of the lateral diffusion constant on membrane microvilli (Wolf et al., 1980). Furthermore, the spatially resolved spectra indicated that the molecular interactions experienced by $DiIC_{16}$ molecules in both the bright and dim areas of the apical plasma membrane were similar. Multispectral imaging did demonstrate, however, that it was possible to readily discriminate between the crystalline and membrane-bound $DiIC_{16}$.

The depletion of cholesterol caused a homogenization of the fluorescence intensity over the apical and basal membrane. Concomitantly, cholesterol depletion greatly reduced the surface ridges on the apical surface, which points to a role for cholesterol in their formation or maintenance. In addition, cholesterol depletion caused the convolutions of the basal membrane and the structure of the lateral membrane to be less complex and the membranes to be smoother in the DIC images. These findings are consistent with a previous report, in which the dose and time dependence of cholesterol depletion in MDCK cells by methyl-β-cyclodextrin is detailed (Francis et al., 1999). Additional investigations of the apical membrane of cholesterol-depleted cells failed to demonstrate any detectable differences in the rate of $DiIC_{16}$ diffusion or in its spectrum. At this point, it is unclear whether the cholesterol depletion directly influences membrane topography or whether it is a secondary effect arising from the interaction of membrane or cytoskeletal proteins with the membrane lipids.

In addition to delineating the basis for the nonuniform fluorescence staining pattern of lipid probes in MDCK cell apical membrane, our experiments confirm previous results about the distribution of lipid probes in the apical and basolateral membranes of epithelia (Dragsten et al., 1982; van Meer and Simons, 1986; Dragsten et al., 1981).

In summary, our investigation shows that, although lipid probes are uniformly distributed in the apical membrane of MDCK cells, they do not produce a uniform pattern of fluorescence. We show that a distinct reticulated fluorescence pattern arises because of geometric rather than chemical or other microenvironmental factors and that the staining pattern of several lipid probes is comparable. The ratio we obtained for the apical surface of MDCK cells, in conjunction with careful analysis of DIC images, can be used as a guide for determining whether the distribution of a given probe is associated with membrane topography or whether it reveals an underlying chemical heterogeneity. Finally, in agreement with Francis et al. (1999), we confirm that there is an important but undefined role for cholesterol in the generation or maintenance of surface microvilli and microridges.

REFERENCES

Aizenbud, B. M., and N. D. Gershon. 1982. Diffusion of molecules on biological membranes of nonplanar form: a theoretical study. *Biophys. J.* 38:287–293.

Andrews, P. M., and K. R. Porter. 1974. A scanning electron microscopic study of the nephron. *Am. J. Anat.* 140:81–115.

Axelrod, D. 1979. Carbocyanine dye orientation in red cell membrane studied by microscopic fluorescence polarization. *Biophys. J.* 26: 557–573.

Axelrod, D., D. E. Koppel, J. Schlessinger, E. Elson, and W. W. Webb. 1976. Mobility measurement by analysis of fluorescence photobleaching recovery kinetics. *Biophys. J.* 16:1055–1069.

Corbeil, D., K. Roper, M. J. Hannah, A. Hellwig, and W. B. Huttner. 1999. Selective localization of the polytopic membrane protein prominin in microvilli of epithelial cells: a combination of apical sorting and retention in plasma membrane protrusions. *J. Cell Sci.* 112:1023–1033.

Crank, J. 1979. The Mathematics of Diffusion. Clarendon Press, Oxford, England

Dragsten, P. R., R. Blumenthal, and J. S. Handler. 1981. Membrane asymmetry in epithelia: is the tight junction a barrier to diffusion in the plasma membrane? *Nature.* 294:718–722.

Dragsten, P. R., J. S. Handler, and R. Blumenthal. 1982. Fluorescent membrane probes and the mechanism of maintenance of cellular asymmetry in epithelia. *Fed. Proc.* 41:48–53.

Francis, S. A., J. M. Kelly, J. McCormack, R. A. Rogers, J. Lai, E. E. Schneeberger, and R. D. Lynch. 1999. Rapid reduction of MDCK cell cholesterol by methyl-β-cyclodextrin alters steady state transepithelial electrical resistance. *Eur. J. Cell Biol.* 78:473–484.

Greenberg, M. L., and D. Axelrod. 1993. Anomalously slow mobility of fluorescent lipid probes in the plasma membrane of the yeast *Saccharomyces cerevisiae*. *J. Membr. Biol.* 131:115–127.

Harris, P. J., J. Y. Chatton, P. H. Tran, P. M. Bungay, and K. R. Spring. 1994. pH, morphology, and diffusion in lateral intercellular spaces of epithelial cell monolayers. *Am. J. Physiol.* 266:C73–C80.

Jacobson, K., and C. Dietrich. 1999. Looking at lipid rafts? *Trends Cell Biol.* 9:87–91.

Kovbasnjuk, O. N., and K. R. Spring. 2000. The apical membrane glycocalyx of MDCK cells. *J. Membr. Biol.* 176:19–29.

Kovbasnjuk, O. N., U. Szmulowicz, and K. R. Spring. 1998. Regulation of the MDCK cell tight junction. *J. Membr. Biol.* 161:93–104.

Roper, K., D. Corbeil, and W. B. Huttner. 2000. Retention of prominin in microvilli reveals distinct cholesterol-based lipid micro-domains in the apical plasma membrane. *Nat. Cell Biol.* 2:582–592.

Scher, M. G., and R. J. Bloch. 1991. The lipid bilayer of acetylcholine receptor clusters of cultured rat myotubes is organized into morphologically distinct domains. *Exp. Cell Res.* 195:79–91.

Snyers, L., E. Umlauf, and R. Prohaska. 1999. Association of stomatin with lipid-protein complexes in the plasma membrane and the endocytic compartment. *Eur. J. Cell Biol.* 78:802–812.

Spring, K. R. 1990. Optical Microscopy for Biology: Proceedings of the International Conference on Video Microscopy Held in Chapel Hill, North Carolina, June 4–7, 1989. B. Herman and K. Jacobson, editors. Wiley-Liss, New York. 513–522.

Spring, K. R. 2000. The use of liquid-crystal tunable filters for fluorescence microscopy. *In* Imaging Neurons: A Laboratory Manual. R. Yuste, F. Lanni, and A. Konnerth, editors. Cold Spring Harbor Laboratory Press, Cold Spring Harbor, NY. 3.1–3.9.

Sund, S. E., J. A. Swanson, and D. Axelrod. 1999. Cell membrane orientation visualized by polarized total internal reflection fluorescence. *Biophys. J.* 77:2266–2283.

Thomas, J. L., D. Holowka, B. Baird, and W. W. Webb. 1994. Large-scale co-aggregation of fluorescent lipid probes with cell surface proteins. *J. Cell Biol.* 125:795–802.

van Meer, G., and K. Simons. 1986. The function of tight junctions in maintaining differences in lipid composition between the apical and the basolateral cell surface domains of MDCK cells. *EMBO J.* 5:1455–1464.

Wolf, D. E. 1985. Determination of the sidedness of carbocyanine dye labeling of membranes. *Biochemistry.* 24:582–586.

Wolf, D. E., M. Edidin, and P. R. Dragsten. 1980. Effect of bleaching light on measurements of lateral diffusion in cell membranes by the fluorescence photobleaching recovery method. *Proc. Natl. Acad. Sci. U.S.A.* 77:2043–2045.